Article citation info:
Ouinten M, Rouabhi R, Herezi A. Power enhancement using grey wolf optimizer algorithm for doubly fed induction generator based on fuzzy logic controller. Diagnostyka. 2026;27(1):2026101. http://dx.doi.org/10.29354/diag/216415.

DIAGNOSTYKA, 2026, Vol. 27, No. 1

e-ISSN 2449-5220
DOI: 10.29354/diag/216415

POWER ENHANCEMENT USING GREY WOLF OPTIMIZER ALGORITHM FOR DOUBLY FED INDUCTION GENERATOR BASED ON FUZZY LOGIC CONTROLLER

Mohammed OUINTEN *, Riyadh ROUABHI, Abdelghafour HERIZI

Department of Electrical Engineering, Faculty of Technology/ LGE Research Laboratory,
Mohamed Boudiaf University of M'sila (28000), Algeria
* Corresponding author, e-mail: mohammed.ouinten@univ-msila.dz

Abstract

The present article investigates innovative control technique for wind energy conversion systems using doubly fed induction generators, accentuating the limitations of conventional proportional-integral controllers under steady-state and variable wind conditions. It examines the integration of nonlinear fuzzy logic controllers to improve robustness, stability, and power quality. Furthermore, a fuzzy grey wolf optimizer algorithm is employed to optimally tune controller gains, optimizing both active and reactive power regulation. The research models the wind turbine, generator, machine and grid-side converters, with MATLAB/Simulink program validating the efficiency of the proposed technique. Results demonstrate that the integrated fuzzy-GWO controller significantly outperforms conventional methods. Specifically, for active power control, it reduces the Integral Time Absolute Error (ITAE) by 98.9% compared to the PI controller and by 95.8% compared to the Fuzzy PD controller. This translates to a faster response with negligible overshoot and superior tracking accuracy under both steady state and variable wind conditions, thereby improving the efficiency and reliability of wind energy systems.

Keywords: power network; doubly fed induction generator; fuzzy logic controller; grey wolf optimizer.

List of Symbols

A	swept surface [m^2];
AC	alternative current;
DC	direct current;
f	viscous friction coefficient;
g	slip;
G	multiplier coefficient;
R	blade radius [m];
V_w	wind speed [m/s];
ρ	air density [kg/m^3];
σ	leakage coefficient;

1. INTRODUCTION

Wind energy is a renewable, clean, and sustainable resource that has historically been used for milling grain, irrigating agricultural fields, and propelling boats. This energy source can significantly contribute to global energy production by reducing fossil fuel consumption, meeting energy demands, and fostering an environmentally friendly society [1][2]. Developed nations are investing in wind energy technologies due to rising fuel prices, consumer demand for electricity, and environmental concerns. Wind power is presently the fastest-expanding source of electrical energy across the globe. [3].

The doubly fed induction generator (DFIG) is an asynchronous electrical machine with a wound rotor design that enables variable-speed operation and efficient energy conversion. For these reasons, DFIGs are widely used in wind farms, providing robust performance, controllable power, reduced noise, and minimal mechanical stress [4][5].

In a DFIG, the stator winding is grid-connected, while the rotor winding is coupled via bidirectional pulse-width modulation converters.

Field oriented control (FOC) is a vector-control technique that controls AC machines by decoupling torque and flux, enabling them to behave similarly to separately excited DC motors [2][3].

The conventional PI controller, widely used in industrial induction-machine applications, benefits from its structure and implementation ease [6]. In practice, gain adjustment is often carried out manually or through trial-and-error procedures, which become labor-intensive and challenging, especially in systems characterized by parameter uncertainties or dynamic operating conditions [7][8][9].

Linear techniques control is often insufficient for achieving desired stability and performance, particularly

Received 2025-05-29; Accepted 2026-01-05; Available online 2026-01-07

due to the inherent non-linearity of the DFIG. Recently, numerous advanced control methods have been suggested to address these challenges [10]. Among these, we have chosen the nonlinear fuzzy logic approach, as it effectively handles uncertainties and significantly improves robustness.

Fuzzy logic controllers (FLCs) are often successfully employed in many complex or non-linear process systems, in certain situations, can achieve better performance than PID controllers [11]. The authors in [12] and [13], utilize FLCs to regulate the machine and grid-side converters in DFIG-based systems, delivering precise performance and stability even during instable wind conditions. This approach facilitates enhanced management of power.

Compared to conventional PI controllers, FLCs exhibit superior robustness, stability, and accuracy in the presence of fluctuating wind speeds [14] [15]. According to studies, FLCs are a favorable choice for maximizing energy conversion in wind systems, as they demonstrate improved stability, reduced overshoot, and compliance with grid code requirements [13] [16] [17].

Although Meta-heuristic algorithms like particle swarm optimization (PSO) [18], genetic algorithms (GA) [19], and ant lion optimizer (ALO) [20] have been successfully applied to DFIG control, the grey wolf optimizer (GWO) offers distinct advantages for this application. As demonstrated in [21], The social hierarchy and hunting strategy of GWO enable a more efficient balance between exploration and exploitation, often leading to faster convergence and a lower probability of settling into local optima compared to PSO and GA. This is critical for tuning the non-linear gains of a fuzzy controller in a high-dimensional search space.

The main contribution of this work resides in the novel synthesis of a Fuzzy PD+I controller structure whose gains are optimally tuned offline using the GWO for decoupled active and reactive power control in a DFIG. While fuzzy logic and metaheuristics have been used separately, the specific application of GWO to this particular hybrid controller is new. The evidence for its innovativeness is demonstrated through its superior performance: it achieves a faster, more accurate, and more robust response compared to the baseline controllers, as quantitatively proven by the significant reduction in performance indices (ITAE, ITSE) and its excellent tracking under a variable wind profile.

This study is presented in this way: section 2 addresses the modeling and control of wind energy system, which incorporates wind turbines, DFIG, machines and grid-side converters. section 3 explains different types of controllers, including fuzzy logic control. In section 4, an overview of the GWO algorithm and the fuzzy-GWO control design is presented. Section 5 exposes results obtained using MATLAB/Simulink, where the controller gains are adjusted by employing the GWO algorithm. These results are analyzed and presented to demonstrate their effectiveness and robustness in regulating both active and reactive power. Finally, the article's conclusion is provided in Section 6.

2. WIND ENERGY SYSTEM MODEL AND CONTROL

WECS is a system that captures a portion of the kinetic energy of the wind and converts it into mechanical energy through a gearbox and then into electrical energy via a generator [22]. Variable-speed turbines are increasingly preferred and are now more common than fixed-speed technologies and provide a significant advantage as they enhance the wind turbine's power output by allowing dynamic rotor speed adjustments. This flexibility results in greater efficiency and energy capture, especially in windy conditions [4]. The model of WECS is illustrated in Fig. 1.

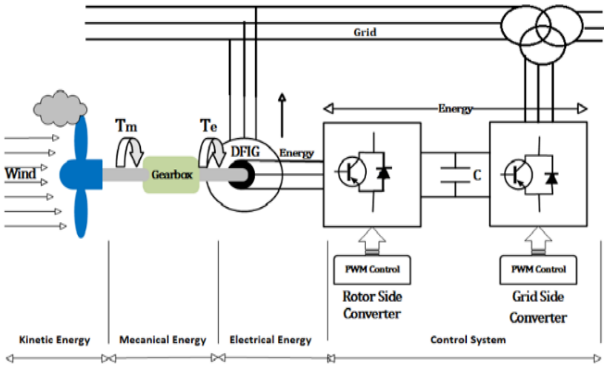

Fig. 1. WECS block diagram

2.1. Wind Turbine Mathematical Model and Control

Wind power is expressed by the Eq. (1):

$$P_w = \frac{1}{2}\rho A V_w^3 \tag{1}$$

With

$$A = \pi R^2 \tag{2}$$

The aerodynamic power produced by the turbine is stated by Eq. (3):

$$P_{aer} = C_P(\lambda,\beta)P_w = \frac{1}{2}C_P(\lambda,\beta)\rho A V_w^3 \tag{3}$$

The power coefficient C_P is a nonlinear function that characterizes the aerodynamic efficiency of the turbine. Its strong dependence on the tip speed ratio λ and the pitch angle β makes the operating point highly sensitive to wind variations, thereby necessitating maximum power point tracking (MPPT) to ensure optimal extraction of power under changing wind conditions.

By definition the tip speed ratio λ is the quotient of the linear speed of the turbine blade tips and the speed of the incoming wind (Eq. 4):

$$\lambda = \frac{R\Omega_t}{V_w} \tag{4}$$

Based on the turbine's aerodynamic model, its behavior exhibits strong nonlinearity and is highly sensitive to wind speed. Fig. 2 illustrates the power–wind speed curve and the corresponding operating

regions of a variable-speed wind turbine, conventionally divided into four zones.

In Zone 1, the turbine is below the cut-in wind speed V_s, and produces no electrical power, as the rotor cannot overcome inherent aerodynamic and mechanical losses.

In Zone 2 corresponds to the variable-speed region, where the extracted power depends directly on the available wind energy. In this zone, the control system adjusts the rotor speed to track the maximum power point.

In Zone 3, once the wind speed reaches the rated value V_n, the turbine operates at a fixed rotational speed to maintain a constant rated power output.

In Zone 4, for wind speeds exceeding the cut-out value V_m, the turbine is disconnected through protective mechanisms to avoid structural overload and ensure the operational safety of the wind energy conversion system (WECS) [23].

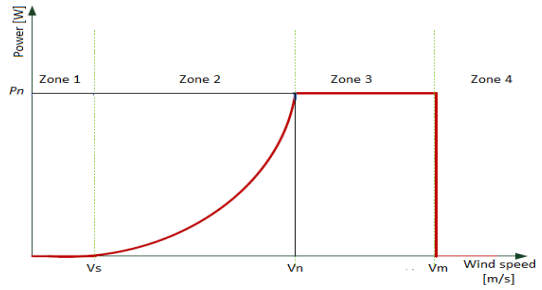

Fig. 2. Characteristics curve

2.1.1. Gearbox Model

The gearbox couples the turbine to the generator, stepping up the low rotational speed of the turbine to the higher speed needed for efficient generator operation (Eq. 5), while concurrently reducing the high shaft torque of the turbine to the lower torque compatible with mechanical limits of the generator (Eq. 6) [24].

$$\Omega_{mec} = G.\Omega_t \tag{5}$$

$$T_g = \frac{T_t}{G} \tag{6}$$

2.1.2. Mechanical Model

The mechanical torque T_{mec} acting on the generator rotor is the summation of the axial torque T_g, the electromagnetic torque T_{em}, and the viscous friction torque T_f (Eq. 7).

$$T_{mec} = J\frac{d\Omega_{mec}}{dt} = T_g - T_{em} - T_f \tag{7}$$

With:

$$T_f = f\Omega_{mec} \tag{8}$$

Based on the equations presented above, the turbine model is represented in Fig. 3.

2.1.3. MPPT Control

Due to the inherently fluctuating and limited nature of wind power, maximum power point tracking algorithms are essential to maintain optimal operating conditions and maximize energy conversion [24]. In Zone 2 of Fig. 2, the MPPT controller dynamically adjusts the electromagnetic torque to extract maximum power under varying wind speeds, while the blade pitch angle remains fixed. The purpose is to optimize energy capture by synchronizing the turbine's mechanical speed with the instantaneous wind velocity. Real-time estimation of wind speed enables this adjustment, allowing the DFIG to operate at its optimal point and ensuring maximum energy efficiency.

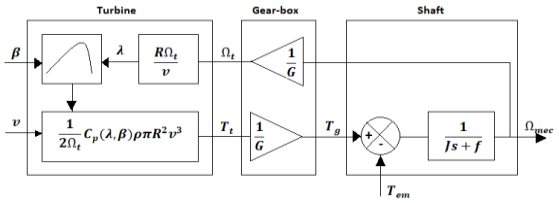

Fig. 3. Wind turbine model

The estimated wind speed's value is provided by Eq.(9):

$$v_{est} = \frac{R.\Omega_t}{\lambda_{opt}} \tag{9}$$

Substituting Eq. (9) into Eq. (3) yields the expression of the reference electromagnetic torque given in Eq. (10):

$$T_{em}^{*} = \frac{1}{2\lambda_{opt}^3} C_{Pmax}\rho\pi R^5\Omega_t^2 \tag{10}$$

The wind turbine model with the MPPT control strategy is depicted in Fig.4.

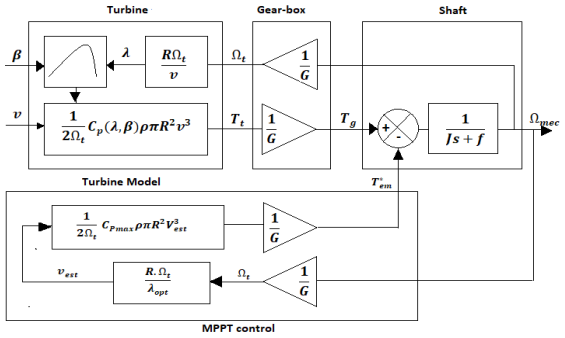

Fig. 4. Wind turbine and MPPT model

2.1.4. Pitch Control

High winds can harm wind turbine mechanics and disrupt electrical system. Pitch control is therefore crucial for optimizing energy extraction and reducing excessive power during gusts, with blades pitched simultaneously or independently for greater system flexibility. Zone 3 in Fig. 2 relates to this control.

2.2. DFIG Mathematical Model and Control

Electrical equations of DFIG is expressed in (Eq.11):

$$\begin{cases} v_{sd} = r_s i_{sd} + \frac{d\varphi_{sd}}{dt} - \omega_s\varphi_{sq} \\ v_{sq} = r_s i_{sq} + \frac{d\varphi_{sq}}{dt} + \omega_s\varphi_{sd} \\ v_{rd} = r_r i_{rd} + \frac{d\varphi_{rd}}{dt} - \omega_r\varphi_{rq} \\ v_{rq} = r_r i_{rq} + \frac{d\varphi_{rq}}{dt} + \omega_r\varphi_{rd} \end{cases} \tag{11}$$

With:

$$\begin{cases} \varphi_{sd} = l_s i_{sd} + l_m i_{rd} \\ \varphi_{sq} = l_s i_{sq} + l_m i_{sq} \\ \varphi_{rd} = l_r i_{rd} + l_m i_{sd} \\ \varphi_{rq} = l_r i_{rq} + l_m i_{sq} \end{cases} \quad (12)$$

Eq. (11), represents the dynamic d-q model of the DFIG in a synchronously rotating reference frame.

The electromagnetic torque is defined by:

$$T_{mec} = \frac{3}{2} p \frac{l_m}{l_s} \left(\varphi_{sq} i_{rd} - \varphi_{sd} i_{rq}\right) \quad (13)$$

The active and reactive powers of the stator are given by:

$$\begin{cases} P_s = v_{sd} i_{sd} + v_{sq} i_{sq} \\ Q_s = v_{sq} i_{sd} - v_{sd} i_{sq} \end{cases} \quad (14)$$

$$\varphi_{sd} = \varphi_s \quad \text{and} \quad \varphi_{sq} = 0 \quad (15)$$

The transformation, Eq. (15), is fundamental to the Field-Oriented Control strategy, as it allows for the decoupling of active and reactive power control, analogous to the independent control of torque and flux in a DC motor.

Additionally, for high-power wind energy conversion machines, the stator resistance r_s is negligible and the DFIG model will be simplified after developing the previous equations, we obtain:

- The torque exerted on the shaft of the generator

$$T_{mec} = -\frac{3}{2} p \frac{l_m V_s}{l_s \omega_s} i_{rq} \quad (16)$$

- The rotor voltages needed to control the generator

$$\begin{cases} v_{rd} = r_r i_{rd} + \sigma l_r \frac{di_{rd}}{dt} - g\omega_s \sigma l_r i_{rq} \\ v_{rq} = r_r i_{rq} + \sigma l_r \frac{di_{rq}}{dt} + g\frac{l_m}{l_s v_s} + g\omega_s \sigma l_r i_{rd} \end{cases} \quad (17)$$

$$\sigma = 1 - \frac{l_m^2}{l_s l_r} \quad (18)$$

- And the active and reactive stator powers injected to the power network:

$$\begin{cases} P_s = -v_s \frac{l_m}{l_s} i_{rq} \\ Q_s = \frac{v_s^2}{l_s \omega_s} - \frac{v_s l_m}{l_s} i_{rd} \end{cases} \quad (19)$$

Fig. 5 illustrates the model of DFIG.

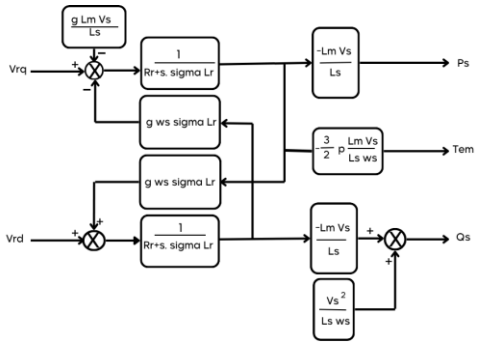

Fig. 5. DFIG model

2.3. Machine-Side Converter Mathematical Model

The DFIG rotor is driven by a two-level inverter that adjusts the bus voltage in order to provide power to the rotor winding and efficiently control state variables. An inverter is a static converter that converts direct current into alternating current. This inverter utilizes semiconductor components like MOSFETs or IGBTs arranged with anti-parallel diodes, incorporating six bi-directional switches (Fig. 6). These switches operate complementarily to maintain phase currents while preventing short-circuiting of the source. In control mode, the inverter functions as a two-position switch, creating two distinct output voltage levels and generating alternating voltage by switching between rectangular pulse outputs. Through regulating rotor speed and reactive power support, the machine-side control maximizes power and delivers an effective steady-state and transient response [25] [26].

The mathematical model of the machine-side converter is given by Eq. (20):

$$\begin{pmatrix} V_a \\ V_b \\ V_c \end{pmatrix} = \frac{E}{6} \begin{pmatrix} 2 & -1 & -1 \\ -1 & -2 & -1 \\ -1 & -1 & -2 \end{pmatrix} \begin{pmatrix} S_1 \\ S_2 \\ S_3 \end{pmatrix} \quad (20)$$

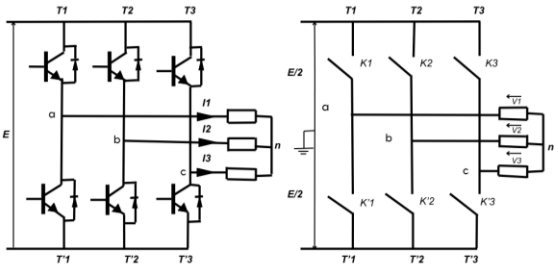

Fig. 6. Machine-side converter

2.4. Grid-Side Converter Mathematical Model and Control

The GSC enables bi-directional power flow from the machine-side converter, keeping the dc-bus voltage stability and ensuring a unity power factor. [25] [26] [27]. It consists of load, converter, and source components. (Fig. 7).

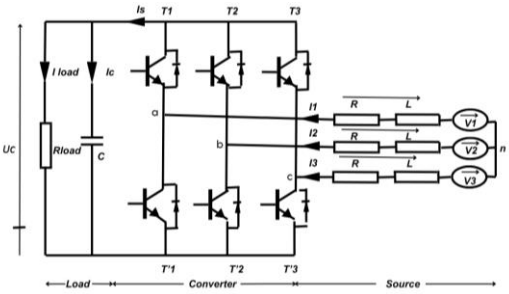

Fig. 7. Grid-side converter

The output voltage is defined by:

$$\begin{cases} U_c = R_{load} I_{load} \\ \frac{dU_c}{dt} = \frac{I_c}{c} = \frac{1}{c}(I_s - I_{load}) \end{cases} \quad (21)$$

The GSC's mathematical model is outlined in Eq.(22):

$$\begin{pmatrix} V_a \\ V_b \\ V_c \end{pmatrix} = \frac{U_c}{3} \begin{pmatrix} 2 & -1 & -1 \\ -1 & 2 & -1 \\ -1 & -1 & 2 \end{pmatrix} \begin{pmatrix} S_1 \\ S_2 \\ S_3 \end{pmatrix} \quad (22)$$

Additionally, the rectified current is stated as follows:

$$I_s = (S_1\ S_2\ S_3)\begin{pmatrix} I_1 \\ I_2 \\ I_3 \end{pmatrix} \quad (23)$$

The state space formulation Eq. (24), represents the AC source model and the rectifier model:

$$\frac{d}{dt}\begin{pmatrix} I_1 \\ I_2 \\ I_3 \end{pmatrix} = \begin{pmatrix} \frac{-R}{L} & 0 & 0 \\ 0 & \frac{-R}{L} & 0 \\ 0 & 0 & \frac{-R}{L} \end{pmatrix}\begin{pmatrix} I_1 \\ I_2 \\ I_3 \end{pmatrix} + \frac{1}{L}\begin{pmatrix} V_1 - V_a \\ V_2 - V_b \\ V_3 - V_c \end{pmatrix} \quad (24)$$

The GSC can be controlled via a sequential management strategy that includes two internal loops for regulating phase current and one external loop for controlling output voltage. According to the subsequent equations, the appropriate voltages and powers in the reference of park transformation are specified:

$$\begin{pmatrix} v_{pd} \\ v_{pq} \end{pmatrix} = \begin{pmatrix} v_d \\ v_q \end{pmatrix} + \begin{pmatrix} -R & L\omega \\ -L\omega & -R \end{pmatrix}\begin{pmatrix} i_d \\ i_q \end{pmatrix} + \begin{pmatrix} -L & 0 \\ 0 & -L \end{pmatrix}\frac{d}{dt}\begin{pmatrix} i_d \\ i_q \end{pmatrix} \quad (25)$$

In below are the expressions for reactive and active power:

$$\begin{pmatrix} P \\ Q \end{pmatrix} = \frac{3}{2}\begin{pmatrix} v_d & v_q \\ v_q & -v_d \end{pmatrix}\begin{pmatrix} i_d \\ i_q \end{pmatrix} \quad (26)$$

3. WIND ENERGY SYSTEM CONCEPTION AND DESIGN

3.1. An Overview of Controllers in WECS

Various kinds of controllers are applied in control systems.

1- Proportional-integral controllers are broadly utilized in regulation of industrial processes due to their simple construction and stable performance across various operating conditions. However, their linear nature makes them less appropriate for mainly nonlinear systems. Fig. 8 illustrates a conventional PI controller, whose transfer function is given by:

$$u(t) = K_p e(t) + K_i \int_0^{\infty} e(\tau)\, d\tau \quad (27)$$

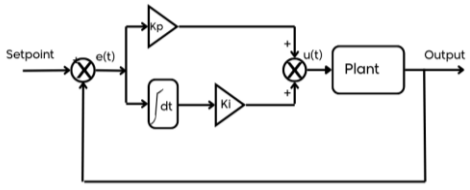

Fig. 8. PI controller

Where $u(t)$), K_p and K_i represent the control input, the proportional gain and the integral gain, respectively, and $e(t)$ designates the difference between the set point and the output of the plant.

Two PI controllers are implemented to adjust the power of the wind system, the first one for active power and the second for reactive power, as shown in Fig. 9.

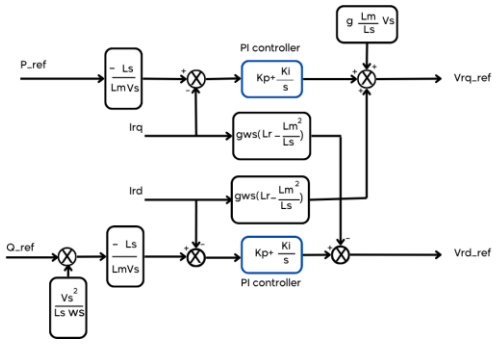

Fig. 9. PI control

2- Fuzzy controller: The fuzzy set theory emerged sixty years ago, and it was first proposed by mathematician Lotfi Zadeh. This theory is a set of rules addressing ambiguous and imprecise knowledge across various systems. Mamdani was the first to implement fuzzy logic in control systems, leading to the widespread application of fuzzy controllers for non-linear and uncertain systems [28].

In the literature, research on fuzzy controllers mainly focuses on two-input systems [29]. Ying uses the error and the rate of error signals as input variables to the fuzzy controller. Fuzzy control is considered as a replacement to PID control. The main types of two-input fuzzy controllers are PD and PI structures:

A Fuzzy-PD controller provides fast dynamic response and good tracking performance, making it suitable for systems requiring rapid changes, though it may suffer from steady-state error and sensitivity to noise due to the derivative term.

Fuzzy-PI controller improves steady-state accuracy and offers smoother control, especially in noisy environments, but typically responds more slowly and may introduce overshoot because of the integral action.

The Fuzzy-PID controller combines the advantages of both, delivering fast response with reduced steady-state error and good robustness, but at the cost of higher complexity in rule design and increased risk of oscillations if not properly tuned [30].

Two fuzzy PD controllers are integrated into the control system, as implemented in Fig. 10, to enhance the tracking of the active and reactive power references.

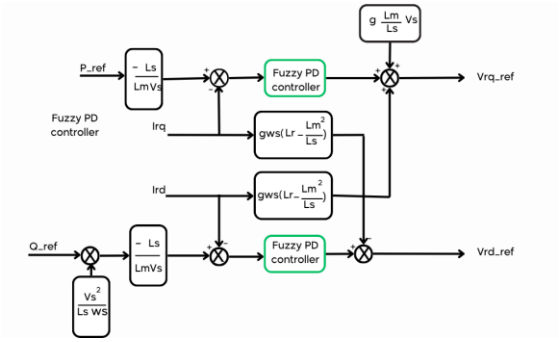

Fig. 10. Fuzzy PD control

3- Fuzzy PD+I controller: The issues mentioned earlier can be resolved by using the fuzzy PD+I controller,

which consists of a fuzzy PD and a linear I controller, as illustrated in Fig. 11.

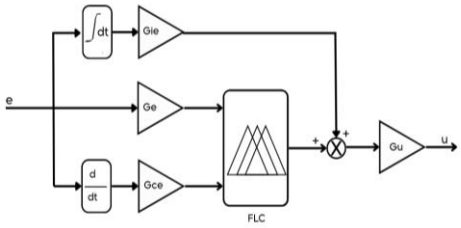

Fig. 11. Fuzzy PD+I controller

In the fuzzy PD+I controller, the fuzzy inference mechanism operates in parallel with the integral action, where the control signal u(t) is obtained by adding the integral term to the output of the fuzzy system. When two fuzzy PD+I controllers are integrated into the wind energy conversion system, the tracking of active and reactive power references is significantly improved, as illustrated in Fig.12.

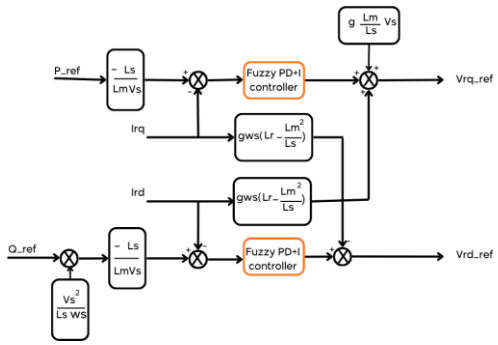

Fig. 12. Fuzzy PD+I control

3.2. Fuzzy Logic Control

Fuzzy logic control relies on a rule-based structure comprising fuzzification, inference, and defuzzification. Membership functions map the input and output variables to linguistic terms, defined using system knowledge, process interpretation, and expert understanding of the system's dynamic behavior. Figs. 13 and 14 illustrate the membership functions of these variables. The error signal uses one triangular and two trapezoidal membership functions, while the rate of error is described by two trapezoidal functions.

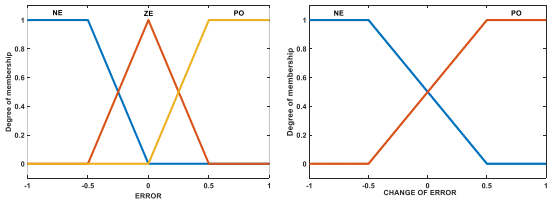

Fig. 13. Membership function for input variables

The number of membership functions for the inputs are intentionally kept minimal to achieve a simple and effective controller, resulting in a compact rule base of only six rules (Table 1). This design reduces computational complexity for potential real-time implementation while still capturing the key nonlinear control actions required for reliable power regulation.

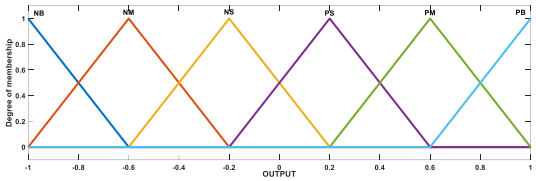

Fig. 14. Membership function for output variable

A Mamdani-type "if–then" inference structure, based on system knowledge and expert experience, is employed. The fuzzy inference uses a simplified product–sum–centroid (gravity) method to further reduce computation and nonlinear effects [31]. Fig.15 illustrates the output surface of the fuzzy PD controller.

Table 1. Fuzzy control rules

de\e	NE	ZE	PO
NE	NB	NM	PS
PO	NS	PM	PB

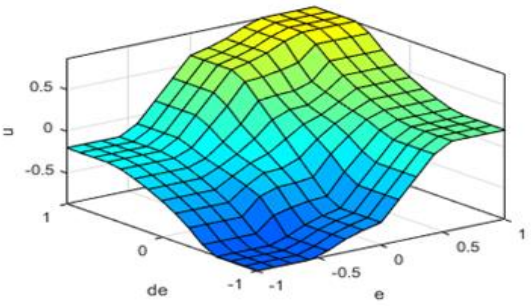

Fig. 15. Structure of FPD+I controller membership function

4. OPTIMIZATION PROCESS

4.1. GWO Concept

In 2014, Mirjalili et al. introduced a meta-heuristic algorithm inspired by grey wolves' social and hunting behaviors. Wolves are categorized into four groups: omega (ω), delta (δ), beta (β), and alpha (α), with the strongest (α, β, δ) guiding (ω) wolves to optimal search areas. [21].

In the social organization, the process considers the best solution as (α), succeeded by (β) and (δ); the remaining are (ω). In the encircling phase, wolves surround prey, mathematically represented through equations that define the distance $(\overrightarrow{l})$ and prey position $(\overrightarrow{y})$ based on coefficient vectors $(\overrightarrow{b})$ and $(\overrightarrow{k})$ as in Eqs. (28, 29) which are derived from random values $(\overrightarrow{r_1})$ *and* $(\overrightarrow{r_2})$ respectively in the interval [0 +1], influencing the movements of the wolves.

$$\vec{l} = \left|\vec{b}.\overrightarrow{y_P}\,(i) - \vec{y}(i)\right| \tag{28}$$

$$\vec{y}(i+1) = \left|\overrightarrow{y_p}(i) - \vec{k}\,.\vec{l}\right| \tag{29}$$

Equations (30, 31) define how the vectors $(\overrightarrow{b})$ and $(\overrightarrow{k})$ are calculated:

$$\vec{k} = 2.\vec{a}.\overrightarrow{r_1} - \vec{a} \quad (30)$$

$$\vec{b} = 2.\overrightarrow{r_2} \quad (31)$$

The coefficient $(\overrightarrow{a})$ decreases linearly from 2 to 0 over the course of the iterations.

The positions of the (α), (β), and (δ) wolves are updated according to Eqs. (35) (36) (37), using the random vectors $(\overrightarrow{k_1})$, $(\overrightarrow{k_2})$, $(\overrightarrow{k_3})$ and the current iteration.

$$\overrightarrow{l_\alpha} = \left|\overrightarrow{b_1}.\overrightarrow{y_\alpha} - \vec{y}\right| \quad (32)$$

$$\overrightarrow{l_\beta} = \left|\overrightarrow{b_2}.\overrightarrow{y_\beta} - \vec{y}\right| \quad (33)$$

$$\overrightarrow{l_\delta} = \left|\overrightarrow{b_3}.\overrightarrow{y_\delta} - \vec{y}\right| \quad (34)$$

$$\overrightarrow{y_1} = \overrightarrow{y_\alpha} - \overrightarrow{k_1}.\overrightarrow{l_\alpha} \quad (35)$$

$$\overrightarrow{y_2} = \overrightarrow{y_\beta} - \overrightarrow{k_2}.\overrightarrow{l_\beta} \quad (36)$$

$$\overrightarrow{y_3} = \overrightarrow{y_\delta} - \overrightarrow{k_3}.\overrightarrow{l_\delta} \quad (37)$$

$$\vec{y}(i+1) = \frac{\overrightarrow{y_1}+\overrightarrow{y_2}+\overrightarrow{y_3}}{3} \quad (38)$$

During the divergence phase, assigning $(\overrightarrow{k})$ a value greater than +1 or less than −1 increase exploration, enabling a broader global search and preventing stagnation in local optima. In the exploitation phase, the wolves focus on the prey by progressively reducing $(\overrightarrow{a})$, which limits the possible range of $(\overrightarrow{k})$ to [-2a +2a]. When $(\overrightarrow{k})$ lies within [−1 +1], the agents shift to a pursuit mode. The overall process is outlined in the flowchart in Fig.16 [21].

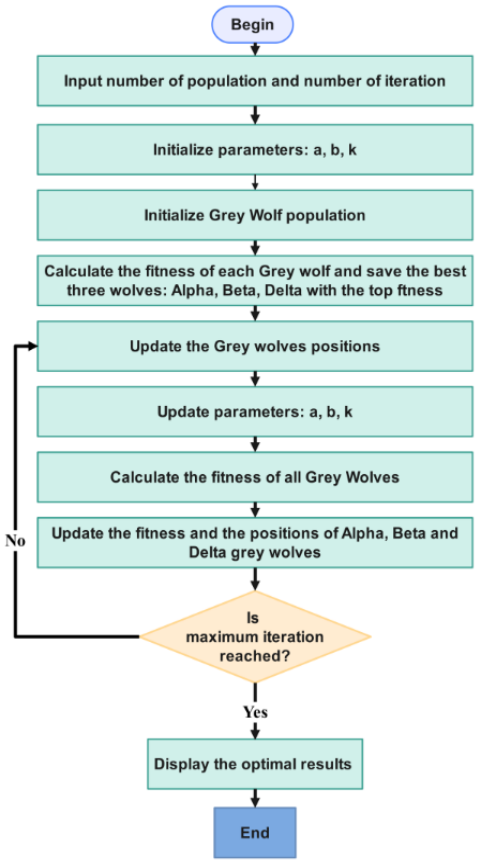

Fig. 16. GWO algorithm flowchart

Several metaheuristic algorithms are applied to optimize controller gains in WECS. In this study, the GWO is adopted due to its reported advantages in the literature. As noted in [21], GWO often exhibits a more efficient balance between exploration and exploitation, achieving faster convergence and reducing the risk of becoming trapped in local minima compared to PSO [18] and GA [19]. This behavior is especially valuable for the high-dimensional, nonlinear optimization involved in tuning the Fuzzy PD+I controller, ensuring robust gains and superior performance, as reflected in the minimal ITAE and ITSE values obtained in our results.

4.2. Optimal Fuzzy Control Using GWO

Notably, the GWO algorithm is executed offline during the design and tuning stage. The purpose is to determine a single optimal set of gains for the fuzzy controllers. Once these gains are obtained, the real-time control loop relies solely on the Fuzzy PD+I controller, whose computational weight is comparable to—and often lower than—that of advanced model-based controllers such as backstepping. This two-stage process (offline optimization followed by online execution) ensures that the proposed approach is well-suited for practical real-time implementation on standard digital signal processors.

Control performance in the DFIG model is determined by the quadrature and direct rotor current components (i_{rq} and i_{rd}), which correspond to active and reactive power. The GWO is employed to minimize the fitness function, improving response time, reducing overshoot, and lowering steady-state errors, with the integral time absolute error (ITAE) serving as the evaluation metric. Fig. 17 illustrates the application of GWO in tuning the proposed fuzzy PD+I controller.

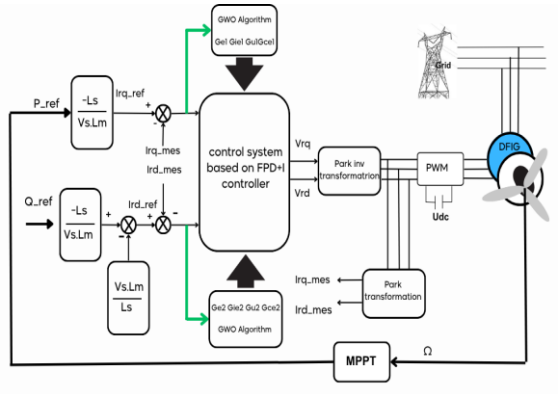

Fig. 17. Fuzzy PD+I-GWO control

5. RESULTS ANALYSIS

5.1. Simulation

In the environment of MATLAB/Simulink, the dynamic behavior of a DFIG linked to the power network and operating at a fixed speed of 1440 revolution per minutes is simulated over a 2-second interval with step changes in power references (a −3000 W step for active power and a +1000 Var step for reactive power). This scenario is designed to thoroughly evaluate the controllers' dynamic response and transient stability.

Furthermore, a second 60-second simulation, carried out under a variable wind profile, lets us to evaluate the performance of the regulators over a longer operational period and representative of real operating conditions. This analysis highlights the ability of controllers to optimize energy capture and maintain satisfactory power quality despite wind fluctuations.

The improved stability and reference tracking directly contribute to enhanced power quality by minimizing fluctuations in active and reactive power, which is crucial for grid stability. While a Total Harmonic Distortion (THD) analysis of the stator current would provide further valuable insight, it falls outside the scope of this particular study which focuses on power-level control. Three types of control are assessed: PI, Fuzzy PD, and Fuzzy PD+I. The characteristics of components of DFIG are presented in Table 2.

Table 2. DFIG Characteristics

Designation	Symbol	Value	Unit
rated power	Pn	5.5	kw
number of pairs of poles	p	2	-
stator rated frequency	f	50	Hz
stator rated voltage	V_s	220/380	V
stator inductance	l_s	0.1554	H
rotor inductance	l_r	0.1568	H
mutual inductance	l_m	0.1500	H
stator resistance	r_s	1.2	Ω
rotor resistance	r_r	1.8	Ω

5.2. Evaluation of Power Tracking

The comparative analysis evaluates the power tracking of the three controllers—PI, Fuzzy PD, and Fuzzy PD+I— using the simulation results illustrated in Figs. 18, 21, and 24. These figures show the reference and actual power trajectories corresponding to each control strategy.

Fig. 18 illustrates the behavior of the PI–GWO controller. Following the step change at t = 0.5 s, the response exhibits a noticeable overshoot and a settling time of about 0.15 s. Although the steady state error remains small, the transient response is slower compared to the fuzzy-based approaches.

Fig. 24 shows the behavior of the suggested Fuzzy PD+I–GWO controller. Unlike the responses observed in Figs. 18 and 21, this controller achieves a near-critically damped behavior, tracking the reference with almost no overshoot and a settling time below 0.05 s. This confirms its superior dynamic performance and greater robustness for sudden changes in energy.

5.3. Performance Index Analysis

The evaluation of the fitness function during the offline GWO optimization for the PI, Fuzzy PD, and Fuzzy PD+I controllers is shown in Figs. 19, 22, and 25. All simulations were performed over a 2-second interval under the specified power conditions. Table3 provides a quantitative comparison. The results confirm that the Fuzzy PD+I–GWO controller achieves the lowest error metrics among all tested strategies. Although direct comparisons with metaheuristics from other studies are limited by differing system configurations, the obtained ITAE value of 0.00179 for active power regulation is highly competitive. In particular, it represents a marked improvement over typical PSO-tuned PI controllers reported for similar DFIG systems [18], highlighting the suitability of GWO for this optimization task.

Table 3. Performance index of active and reactive power

Power	Index criteria	PI-GWO	FPD-GWO	FPD+I-GWO
Active	ise	20.98	0.13620	0.00674
	iae	1.459	0.18300	0.00274
	itse	0.996	0.01523	0.00654
	itae	0.162	0.04281	0.00179
Reactive	ise	21.52	1.17700	0.00999
	iae	1.424	0.36470	0.00361
	itse	0.659	0.03163	0.00102
	itae	0.113	0.03910	0.00093

Table 4. Optimal gains of controllers

Power	Gain	PI-GWO	FPD-GWO	FPD+I-GWO
Active	Ge1	3.855	9.00E-05	3.83E-07
	Gie1	478.8	-----	7.26E+1
	Gce1	-----	4.04E-06	5.47E-08
	Gu1	-----	29977814	1.14E+05
Reactive	Ge2	3.903	1.00E-4	7.52E-07
	Gie2	364.1	----	7.75E+01
	Gce2	----	5.35E-06	5.92E-08
	Gu2	----	29933834.6	1.14E+05

5.4. Gains Optimization Results

The GWO algorithm is applied offline to optimize the gains of each controller type individually. It is configured with a population of 10 grey wolves and a maximum of 100 iterations; however, the gain trajectories converge rapidly, typically in less than 100 iterations. Figs. 20, 23, and 26 illustrate the gain evolution for the PI, fuzzy PD, and fuzzy PD+I controllers, respectively. Table 4 reports the resulting optimal gains, which provide improved dynamic performance and ensure stable system operation.

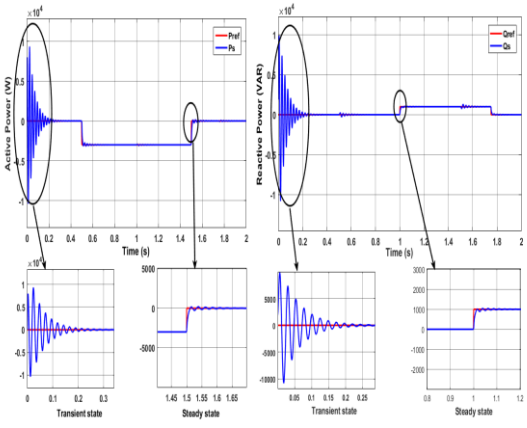

Fig. 18. PI-GWO control of stator power at steady wind speed

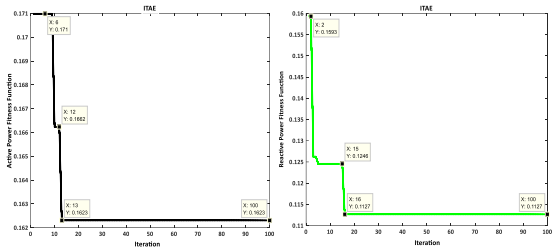

Fig. 19. PI--GWO controller performance evaluation during simulation

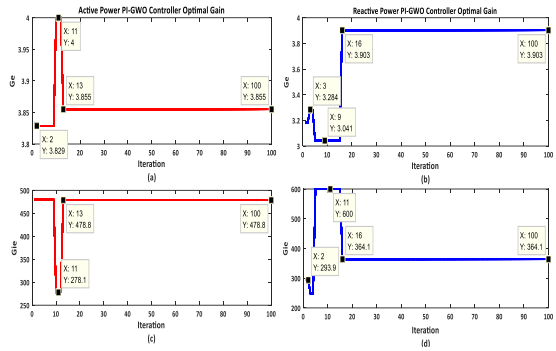

Fig. 20. Variations in PI-GWO controller gains during simulation

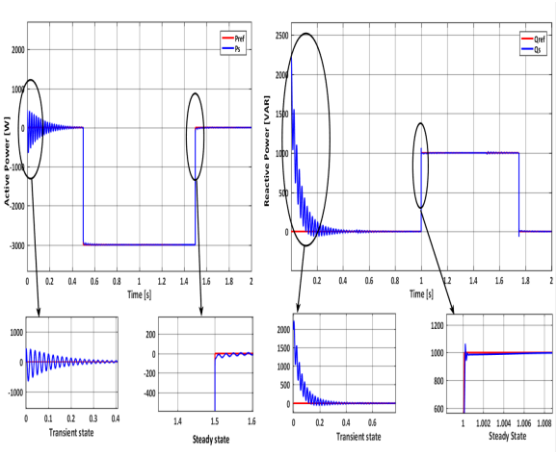

Fig. 21. FPD-GWO control of stator power at steady wind speed

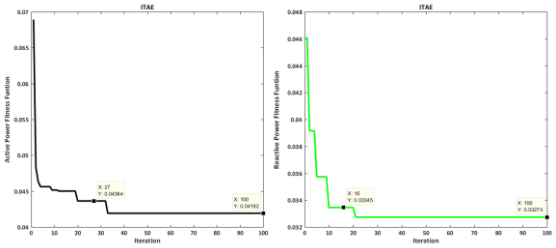

Fig. 22. FDP-GWO controller performance evaluation during simulation

5.5. Dynamic Control of Power at Variable Wind Speeds

To validate the controller's performance under a main challenge in wind energy systems—highly variable wind speeds—a 60-second simulation was conducted using a variable wind profile. Fig. 27 presents the expected and measured values of the stator power. The results demonstrate that the proposed Fuzzy PD+I-GWO controller maintains superior tracking accuracy and stability even under these realistic and fluctuating conditions, effectively maximizing energy extraction in the second operational zone (Fig. 2) and ensuring stable power delivery.

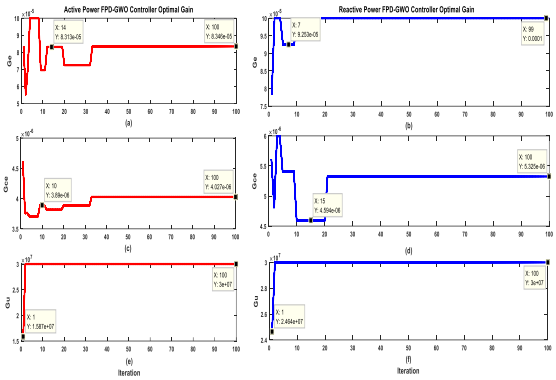

Fig. 23. Variations in FPD-GWO controller gains during simulation

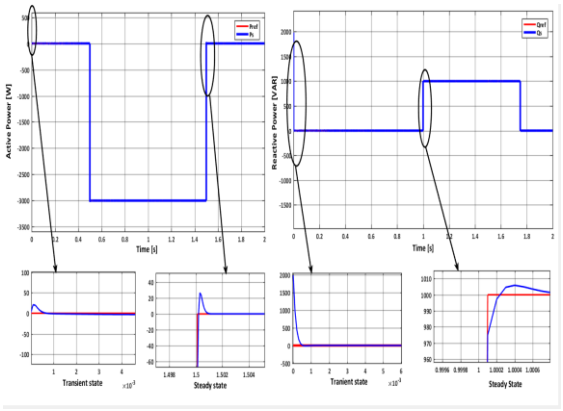

Fig. 24. FPD+I-GWO control of stator power at steady wind speed

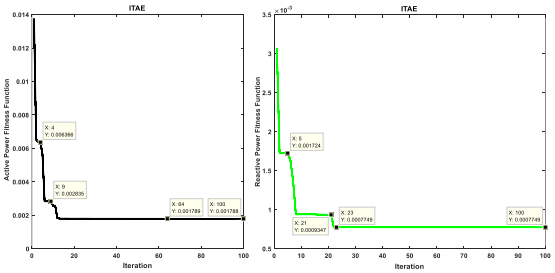

Fig. 25. FDP+I-GWO controller performance evaluation during simulation

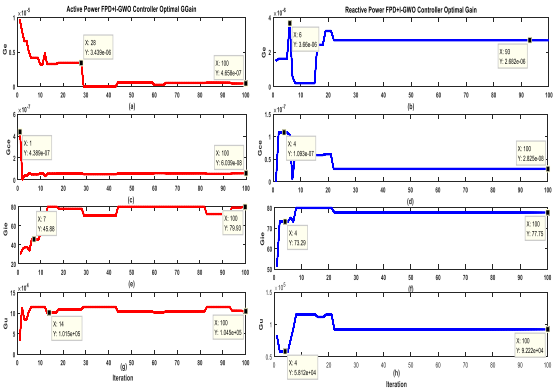

Fig. 26. Variations in FPD+I-GWO controller gains during simulation

5.6. Comparative Discussion and Broader Applicability

The proposed Fuzzy–GWO control strategy offers a practical and efficient alternative to other advanced controllers. Unlike adaptive fuzzy, neural adaptive, or MPC-based methods [32] [33], which require continuous online optimization and thus incur computational cost and potential stability concerns, our approach performs all optimization offline. This results in a fixed-gain fuzzy controller that is simple to deploy in real time while retaining strong robustness to nonlinearities, parameter variations, and variable wind conditions (Fig. 27).

Compared with techniques such as Sliding Mode Control—known for chattering issues—or Adaptive Backstepping and other model-dependent strategies [10] [20], which rely on accurate system modeling and often lead to complex laws, the Fuzzy–GWO framework remains model-free, smooth, and easy to implement. Its dynamic performance, including sub-0.05 s settling time and negligible overshoot (Fig. 24), is competitive with PSO-based optimization approaches [18] while avoiding the need for online computation.

Beyond wind energy, the same hybrid control–optimization concept is well suited to other nonlinear and uncertain systems. Examples include high-precision trajectory tracking in robotic manipulators [34], advanced motor–compressor drives [35], and power-quality management in microgrids, highlighting its potential for broader technological impact.

5.7. Discussion on Robustness and Sensitivity

The higher performance of the Fuzzy PD+I-GWO controller, as quantified by the lowest ITAE and ITSE values in Table 3, demonstrates not only precision but also inherent robustness. The low steady-state error and minimal overshoot indicate that the GWO-optimized gains provide a stable and resilient control law that is less sensitive to the system's non-linearities and the step changes in power reference. Furthermore, the controller's ability to maintain excellent tracking performance under variable wind speed conditions, as shown in Fig. 27, reflects the controller's robustness in the presence of operational disturbances and parameter changes, a challenge that often affects linear PI controllers.

6. CONCLUSIONS

This study successfully developed and validated a hybrid fuzzy PD+I controller with gains optimally tuned using the GWO for a DFIG-based wind energy system. The suggested strategy significantly improves power tracking performance compared to conventional and simpler fuzzy controllers. Its practical impact lies in the potential to enhance energy yield and grid stability in wind farms through more responsive and stable control.

Simulation results demonstrate the superiority of the fuzzy PD+I–GWO controller in a high-fidelity software environment, including robustness to reference changes and wind speed variations.

The research leads to several key findings:

GWO is highly effective for offline tuning of fuzzy controller gains in complex, nonlinear systems like the DFIG.

The fuzzy PD+I controller optimized with GWO achieves faster response (settling time < 0.05 s), lower steady-state error, and negligible overshoot compared to GWO-tuned PI and fuzzy PD controllers.

Quantitative improvements are evidenced by a dramatic reduction in performance indices, with ITAE reduced by over 98% relative to PI control.

The controller maintains superior performance and stability under variable wind speed profiles, demonstrating its applied feasibility and robustness.

Future work will concentrate on real-time implementation using digital controllers, validation via hardware-in-the-loop (HIL) test benches or physical prototypes, and evaluation under practical challenges

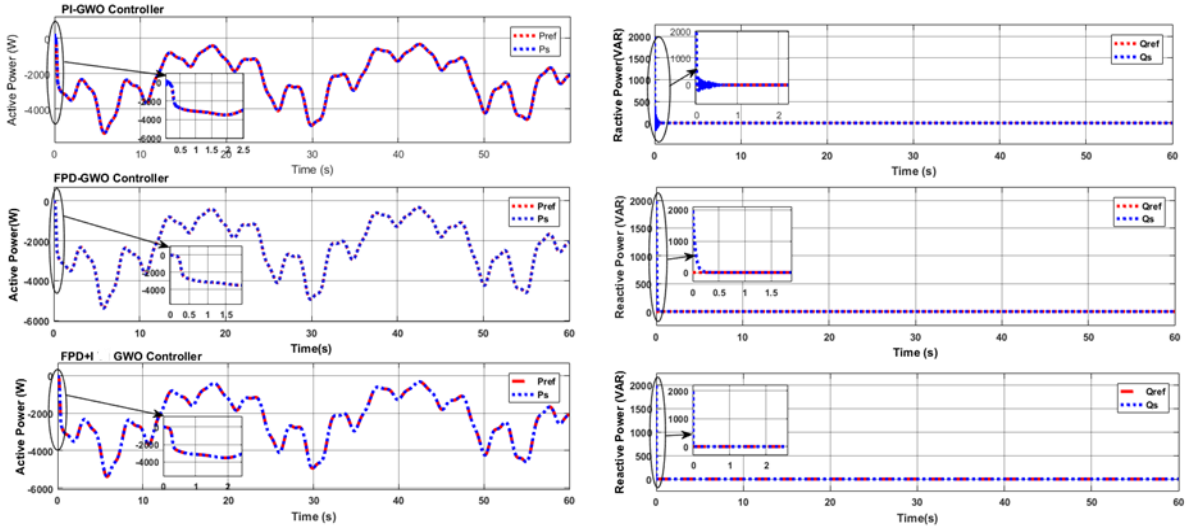

Fig. 27. DFIG power simulation at variable speed for PI-GWO, FPD-GWO and FPD+I-GWO controllers

such as grid voltage sags, measurement noise, and parameter variations (e.g., stator/rotor resistance and inductance) to fully quantify robustness.

Source of funding: *This research did not receive any outside financial support.*

Authors contributions: *Research concept and design, M.O.; Collection and/or assembly of data, M.O.; Data analysis and interpretation, M.O., A.H.; Writing the article, M.O.; Critical revision of the article, R.R., A.H.; Final approval of the article, R.R.*

Declaration of competing interest: *The author declares no conflict of interest.*

REFERENCES

1. Zhang S, Robinson E, Basu M. Hybrid Gaussian process regression and Fuzzy Inference System based approach for condition monitoring at the rotor side of a doubly fed induction generator. Elsevier, Renewable Energy. 2022;198:936-946. http://dx.doi.org/10.1016/j.renene.2022.08.080.
2. Bouderbala M, Bossoufi B, Lagrioui A, Taoussi M, Aroussi H. A, Ihedrane Y. Direct and indirect vector control of a doubly fed induction generator based in a wind energy conversion system. International Journal of Electrical and Computer Engineering (IJECE). 2018;9(3):31-1540. http://dx.doi.org/10.11591/ijece. v9i3.
3. Soloumah Hany M. Jabr. Doubly-fed induction generator used in wind energy. Doctoral Thesis, University of Windsor, Windsor, Ontario, Canada 2008.
4. Ofualagba G, Ubeku EU. Wind energy conversion system- wind turbine modeling. IEEE Power and Energy Society General Meeting - Conversion and Delivery of Electrical Energy in the 21st Century Pittsburgh, PA, USA 2008:1-8. http://dx.doi.org/10.1109/PES.2008.4596699.
5. Mouhi N. E, Essadki A. Active and Reactive Power Control of DFIG used in WECS using PI Controller and Backstepping. International Renewable and Sustainable Energy Conference (IRSEC) Tangier Morocco 2017:1-6. http://dx.doi.org/10.1109/IRSEC.2017.8477349.
6. Zoubir Z, Linda B, Abdelkader L. Field oriented control of doubly fed induction generator integrated in wind energy conversion system using artificial neural networks. International Conference on Electrical Sciences and Technologies in Maghreb (CISTEM). 2018:1-7. http://dx.doi.org/10.1109/CISTEM.2018.8613558.
7. Bahgaat NK, Moustafa Hassan MA. Swarm intelligence PID controller tuning for AVR System. In: Azar A, Vaidyanathan S. (eds) Advances in Chaos Theory and Intelligent Control. Studies in Fuzziness and Soft Computing, Springer, Cham, 2016; 337:791-804. http://dx.doi.org/10.1007/978-3-319-30340-6_33.
8. Reddy K, Saha A. K. A review of swarm based metaheuristic optimization techniques and their application to doubly fed induction generator. Heliyon. 2022;8(10):01–33. http://dx.doi.org/10.1016/j.heliyon. 2022.e10956.
9. Supriya GV, Reddy MR, Kumar PB. Optimal tuning of PID controller parameters for AGC of a wind integrated interconnected power system. ITEGAM-JETIA, Manaus. 2024;10(46): 33-41. http://dx.doi.org/10.5935/jetia. v10i46.1095.
10. Moumani Y, Laafou A. J, Ait Madi A. Modeling and Backstepping Control of DFIG used in Wind Enegry Conversion System. 7th International Conference on Optimization and Applications (ICOA), Wolfenbüttel, Germany. 2021:1-6. http://dx.doi.org/10.1109/ICOA51614.2021.9442625.
11. Saeed BI, Mehrdadi B. Zero overshoot and fast transient response using a fuzzy logic controller. The 17th International Conference on Automation and Computing, Huddersfield, UK, 2012:116-120.
12. Malathi P. Fuzzy logic controller for doubly fed induction generator based wind energy conversion system. International Journal of Advanced Trends in Engineering and Management (IJATEM). 2024;3(06):41-51. http://dx.doi.org/10.59544/dvau7154/ijatemv03i06p5.
13. Kebede M, Tuka M. Power control of wind energy conversion system with doubly fed induction generator. Journal of Energy, 2022: 01-12. http://dx.doi.org/10.1155/2022/8679053.
14. Rached B, Elharoussi M, Abdelmounim E. Design and investigations of MPPT strategies for a wind energy conversion system based on doubly fed induction generator. International Journal of Electrical and Computer Engineering (IJECE). 2020;10(5): 4770-4781. http://dx.doi.org/10.11591/IJECE.V10I5.PP4770-4781.
15. Hemeyine AV, Abbou A, Bakouri A, Mokhlis M, El Moustapha SM. A robust interval Type-2 fuzzy logic controller for variable speed wind turbines based on a doubly fed induction generator. Inventions. 2021;6(21):1–14. http://dx.doi.org/10.3390/inventions6020021.
16. Haile EA, Worku GB, Beyene AM, Tuka MB. Modeling of doubly fed induction generator based wind energy conversion system and speed controller. Journal of Energy Systems. 2021:46-59. http://dx.doi.org/10.30521/jes.854669.
17. Bounifli F, Wahabi A, Elmoudden A. The modeling of the wind system and contribution to the control of doubly-fed induction generator with using fuzzy logic. International Journal of Innovations in Engineering and Technology (IJIET). 2017;8(2):311-318. http://dx.doi.org/10.21172/ijiet.82.045.
18. Bekakra Y, Ben Attous D. Optimal tuning of PI controller using PSO optimization for indirect power control for DFIG based wind turbine with MPPT. International Journal of System Assurance Engineering and Management, July-Sept 2014; 5(3): 219–229. http://dx.doi.org/10.1007/s13198-013-0150-0.
19. Guediri A, Hettiri M, Guediri A. Modeling of a wind power system using the genetic algorithm based on a doubly fed induction generator for the supply of power to the electrical grid. Processes. 2023;11(952):01–19. http://dx.doi.org/10.3390/pr11030952.
20. Zeghdi Z, Barazane L, Bekakra Y. Improved backstepping control of a dfig based wind energy conversion system using ant lion optimizer algorithm. Periodica Polytechnica Electrical Engineering and Computer Science. 2022; 66(1):43–59. http://dx.doi.org/10.3311/PPee.18716.

21. Mirjalili S, Mirjalili S. M, Lewis A. Grey wolf optimizer. Elsevier, Advances in Engineering Software. 2014;69:46–61. http://dx.doi.org/10.1016/j.advengsoft.2013.12.007.
22. Karimi M, Zekraoui M, Khaouch Z, Touairi S. Intelligent vector control for a novel mechatronic modeling of a 1.5MW variable speed WECS using the bicausality concept under a real wind flow: A Bond Graph Approach. Franklin Open. 2024:01-14. http://dx.doi.org/10.1016/j.fraope.2024.100129.
23. Mensou S, Essadki A, Nasser T, Idrissi BB, Tarla LB. Dspace DS1104 implementation of a robust nonlinear controller applied for DFIG driven by wind turbine. Renewable Energy. 2020;147:1759–1771. http://dx.doi.org/10.1016/j.renene.2019.09.042.
24. Chojaa H, Derouich A, Zamzoum O, Watil A, Taoussi M, Abdelaziz Al Moataz Y, Elbarbary ZMS, Mossa MA. Robust control of DFIG-Based WECS integrating an energy storage system with intelligent MPPT under a real wind profile. IEEE Access. 2023;11:90065–90083. http://dx.doi.org/10.1109/ACCESS.2023.3306722.
25. Rouabhi R, Herizi A, Djerioui A. Performance of robust type-2 fuzzy sliding mode control compared to various conventional controls of doubly-fed induction generator for wind power conversion systems. Energies. 2024;17(3778):01–24. http://dx.doi.org/10.3390/en17153778
26. Rouabhi R, Zemmit A, Herizi A, Moussa, Djeriou O. Hybrid type-2 fuzzy backstepping control of doubly fed induction generator for wind energy conversion systems. Journal of the Brazilian Society of Mechanical Sciences and Engineering. 2025;47:24:1-20. http://dx.doi.org/10.1007/s40430-024-05293-z.
27. Lagudu VSK, Ananth DVN, Madichetty S. Independent control of active and reactive power for grid connected DFIG using reference power based improved field-oriented control scheme. International Journal of Ambient Energy. 2020:01-20. http://dx.doi.org/10.1080/01430750.2020.1818123.
28. Pichan M, Rastegar H, Monfared M. Two fuzzy-based direct power control strategies for doubly-fed induction generators in wind energy conversion systems. Energy. 2013;51(1):154-162. http://dx.doi.org/10.1016/J.ENERGY.2012.12.047.
29. Eker I, Torun Y. Fuzzy logic control to be conventional method. Elsevier, Energy Conversion and Management. 2006;47(4):377-394. http://dx.doi.org/10.1016/j.enconman.2005.05.008.
30. Kim BJ, Chung CC. Design of fuzzy PD + I controller for tracking control. IEEE Proceedings of the American Control Conference, Anchorage. 2002;3: 2124-2129. http://dx.doi.org/10.1109/ACC.2002.1023950.
31. Tabatabaei S, Barzegar A, Sadeghi MS, Roosta P. Fuzzy PD+I and Fuzzy PID controllers design for a nonlinear quarter car suspension system. International Conference on Computer Applications and Industrial Electronics (ICCAIE 2010), Kuala Lumpur, Malaysia. 2010:186-190. http://dx.doi.org/10.1109/ICCAIE.2010.5735072.
32. Zouari F, Saad KB, Benrejeb M. Robust neural adaptive control for a class of uncertain nonlinear complex dynamical multivariable systems. International Review on Modelling and Simulations. 2012;5(5):2075-2103.
33. Boulkroune A, Zouari F, Boubellouta A. Adaptive fuzzy control for practical fixed-time synchronization of fractional-order chaotic systems. Journal of Vibration and Control. 2025;0(0). https://doi:10.1177/10775463251320258.
34. Zouari F, Saad KB, Benrejeb M. Adaptive backstepping control for a single-link flexible robot manipulator driven DC motor. In 2013 International Conference on Control, Decision and Information Technologies (CoDIT). 2013;864-871.
35. Rigatos G, Abbaszadeh M, Sari B, Siano P, Cuccurullo G, Zouari F. Nonlinear optimal control for a gas compressor driven by an induction motor. Results in Control and Optimization. Volume 2023;11:100226. https://doi.org/10.1016/j.rico.2023.100226.

Mohammed OUINTEN doctorate student at M'sila University. Obtained the Master Degree in electrical engineering, from University of Ghardaia, Algeria in 2021. His current research area includes the control of doubly-fed induction machines using algorithm.
Email: mohammed.ouinten@univ-msila.dz

Dr. **Riyadh ROUABHI** works in the Department of Electrical Engineering at M'sila University. Obtained the Ph.D. Degree in electrical engineering, from university of Batna, Algeria in 2016. His current research area includes the control of induction machines and renewable energy.
Email: riyadh.rouabhi@univ-msila.dz

Dr. **Abdelghafour HERIZI** graduated with a degree in electronic engineering in 2006 from the University of M'sila in Algeria, and two years later, he earned a magister degree in electrical engineering from the Polytechnic Military School in Algiers. In 2021, the University of M'sila will award the Ph.D. in electrical engineering. He is currently Principal Investigator at the Electrical Engineering Laboratory, University of M'sila. His research interests include the modelling and control for nonlinear systems and renewable energy.
Email: abdelghafour.herizi@univ-msila.dz